Supporting Information (SI Appendix):

Warning Signals for Eruptive Events in Spreading Fires

Jerome M. Fox and George M. Whitesides

[1]Department of Chemistry and Chemical Biology, Harvard University, Cambridge, MA 02138, USA.
[2]Wyss Institute for Biologically Inspired Engineering, Harvard University, Cambridge, MA 02138, USA.
[3]The Kavli Institute for Bionano Science and Technology, Harvard University, Cambridge, MA 02138, USA.
*To whom correspondence should be addressed. E-mail: gwhitesides@gmwgroup.harvard.edu

SI Methods

Experimental Setup. We constructed our model system by placing strips of nitrocellulose (VWR, Nitrocellulose Membrane BA83, 0.2 μm pore size) onto a suspended wire mesh and igniting them from one end (the material of this mesh did not, via conduction, influence rates of propagation for structured and unstructured flames; see SI Note 1). By imaging the propagation of flames along these strips, we examined structured and unstructured propagation behaviors (and transitions between them). The particular brand of nitrocellulose that we employed was electrostatically charged and, thus, stuck to the surface of wire mesh. To ensure adequate airflow to the bottom of burning strips, we separated the wire mesh from a glass surface by a 2.5-cm gap (Fig. S1A). To prevent stray currents of air from interfering with spread behaviors, we placed the paper/mesh setup in an enclosed fume hood with no airflow (Fig. S1B).

The meshes employed in this study consisted of two sizes (McMaster-Carr): a small mesh, which contained diamond-shaped holes with areas of 0.051 cm^2 and an areal density of 5 holes/cm^2; and a large mesh, which contained diamond-shaped holes with areas of 0.13 cm^2 and an areal density of 2 holes/cm^2. We used the large mesh for all experiments except those indicated (e.g., Table S1). Unless we have indicated otherwise, we carried out all experiments in ambient laboratory conditions maintained at 20° +/- 2° C and 12% +/- 2% relative humidity (RH) by the building environmental controls. For the high-temperature experiments (Table S1, Fig. S9C), the large mesh was supported by two hot plates; reported temperatures indicate the temperatures of nitrocellulose strips placed in the center of the mesh, between the two plates. Temperatures were measured with a Raytek Raynger ST infrared thermometer.

Imaging. We imaged propagating flames with a combination of high-speed (Phantom V310), thermal (FLIR), and digital (Nikon D1500) photography. For high-speed imaging, we used a

capture speed of 7000 frames/second and an exposure time of 114 μs. (Note: the high-speed camera was fitted with a Zeiss Planar 85 mm f/1.4 ZF.2 lens with aperture f/4). For thermal and digital images, we used automatic exposure and focusing. Still images of high-speed videos in which flames moved from right to left were flipped to show flames moving from left to right.

Measurement of Combustion Rates. To quantify rates of combustion associated with each regime, we measured the time required for a propagating flame to travel specified distances (12-20 cm) by using (i) video collected by a camera (Nikon D1500) placed directly above the wire mesh, (ii) a digital timer, and (iii) Equation S1, where ρ_{strip} is the density of the strip (~ 4.9 mg/cm^2), v is the velocity of the flame (cm/s), and w_{strip} is the width of the strip (cm).

$$Rate\ of\ combustion = \rho_{strip} \cdot v \cdot w_{strip} \qquad \text{(S1)}$$

To measure rates of propagation in the unstructured regime, we triggered early structured-to-unstructured transitions by placing a bump (1-cm inverted "V") at a distance of 4 cm from the ignition end of the strip; these early transitions allowed us to image unstructured flames propagating along 20-cm distances. In Figure 2A, each data point represents an average rate of combustion calculated from at least five individual experiments.

For strips positioned at steep angles (Fig. 3B), unstructured flames moved too quickly for the accurate determination of velocities with the Nikon D1500 camera. Thus, to calculate all rates of combustion shown in Fig. 3B, we employed a high-speed camera (Phantom V310). Each data point for structured flames corresponds to the average rate of combustion calculated from at least 7 individual experiments; each data point for unstructured flames, which exhibited greater variability in velocity than structured flames, corresponds to the average rate of combustion calculated from at least 15 individual experiments.

Probabilities of Transitions. We calculated values of P_{SU} and P_{US} for different sets of conditions (e.g., Figs. 3A and 4C) by employing the same general formula: for a particular contour and set of conditions, we counted the number of contour-initiated transitions, and then calculated P_{SU}, the probability of a structured-to-unstructured transition, or P_{US}, the probability an unstructured-to-structured transition, by employing Equation S2, where n_{trans} is the number of successful transitions, and n is the total number of experiments ($n \geq 25$ for this study).

$$P = \frac{n_{trans}}{n} \qquad \text{(S2)}$$

We calculated probabilities associated with structured-to-unstructured transitions by examining the propagation of structured flames along 30-cm strips of nitrocellulose with bumps located 15 cm from their extinction end (e.g., for strips containing bumps shaped like an inverted "V", those bumps were placed 15 cm from the point of extinction and, thus, 13 cm from the point of ignition). We calculated probabilities associated with unstructured-to-structured transitions by examining the propagation of unstructured flames along 30-cm strips of nitrocellulose with bumps located 4 cm from the ignition end of the strip (to initiate the unstructured flame) and 8 cm from the extinction end of the strip (to trigger the unstructured-to-structured transition).

Reproducibility of Measurements. Ignited nitrocellulose burned in a highly reproducible manner. The relative standard deviation (i.e., the standard deviation divided by the mean) of measured rates of combustion was 7% for structured flames and 12% for unstructured flames (Table S2), and trends in P_{SU} for strips of different widths were similar between different batches of nitrocellulose (Fig. S9A). In Figure S9A batches of nitrocellulose are as follows: batch 1 (VWR BA 83 Nitrocellulose: CAST No. / CONV No. = G4329137 / G5053136 and G4329137 / G5053136) and batch 2 (VWR BA 83 Nitrocellulose: CAST No. / CONV No = G5153140 / G6017141 and G5913141 / G6130136).

Calculation of Mean Apparent Brightness (B_{ap}). We examined dynamics of our system by monitoring the temporal evolution of the mean apparent brightness (B_{ap}) for successive high-speed images. To evaluate values of B_{ap}, we wrote a MATLAB program that carries out the following steps: (i) it calculates the mean values of red, green, and blue pixel intensities (I_{red}, I_{green}, and I_{blue}, respectively) within the 512x512 uint8 matrix describing those intensities for each image; (ii) it calculates B_{ap} by adding those values together ($B_{ap} = I_{red} + I_{green} + I_{blue}$); (iii) it carries out (i) and (ii) for successive frames; (iv) it calculates the matrix of (t, B_{ap}) pairs and plots them as shown in Fig. 4B and Figs. S10-S11.

To examine the relationship between B_{ap} and the size of a flame, we carried out the following steps: (i) we used a high-speed camera to image the front of propagating flames supported by strips of different widths (we note, the camera was positioned ~1 m away from the propagating flames); (ii) we used high-speed images of those flames to estimate width and height; (iii) we estimated the area of each flame by approximating them as ellipses; and (iv) we calculated B_{ap} for each flame by using the procedure detailed in the proceeding paragraph. Figure S3, which shows the dependence of B_{ap} on flame area, suggests that B_{ap} is a linear function of the area of a flame. (We note: for a particular setup, the slope of the line relating B_{ap} to flame area depends on the distance of the flame from the high-speed camera.)

Statistical Indicators of Slowing Down. To evaluate commonly proposed statistical indicators of critical slowing down, we calculated the variance, lag-1 autocorrelation, and skewness of B_{ap} for structured flames propagating along strips positioned at different angles relative to a level surface (θ_{strip}). In order to examine patterns in behavior that emerge as structured-to-unstructured transitions become more likely, we chose angles within the bistable region (Fig. 2C) located at different proximities to $\theta_{strip} = 115°$ (the structured-to-unstructured bifurcation point).

To carry out the required calculations, we wrote a MATLAB program that implemented the operations described below for 7000 frames (1 second) within ten separate videos at each angle (i.e., for each data point in Fig. 4A).

Variance: The program calculated the variance of B_{ap} (a measure of the spread of B_{ap} about the sample mean) by implementing Equation 1, where n is the total number of frames (7000), B_i is the mean apparent brightness of frame i, and $\bar{B}$ is the mean apparent brightness of all 7000 frames.

$$Var(B_{ap}) = \frac{1}{n-1}\sum_{i=1}^{n}(B_i - \bar{B})^2 \quad (1)$$

Lag-1: The program calculated the lag-1 autocorrelation (Lag-1 AC; a measure of the self-similarity of B_{ap} over time) by implementing Equation 2 (*1*), where n is the size of the window (n=7000), B_i is the brightness of frame i, and $\bar{B}$ is the mean apparent brightness of all 7000 frames.

$$Lag_1\ AC(B_{ap}) = \frac{\frac{1}{n}\sum_{i=1}^{n-1}(B_i-\bar{B})(B_{i+1}-\bar{B})}{\frac{1}{n-1}\sum_{i=1}^{n}(B_i-\bar{B})^2} \quad (2)$$

Skewness: The program calculated the skewness of B_{ap} (a measure of the asymmetry in the distribution of B_{ap} about the mean) by implementing Equation 3, where B_i is the mean apparent brightness of frame i, and $\bar{B}$ is the mean apparent brightness of all 7000 frames.

$$Skewness(B_{ap}) = \frac{\frac{1}{n}\sum_{i=1}^{n}(B_i-\bar{B})^3}{\left(\sqrt{\frac{1}{n}\sum_{i=1}^{n}(B_i-\bar{B})^2}\right)^3} \quad (3)$$

Behavioral Indicators of Slowing Down. To estimate values of $t_{recovery}$, the time between the end of an encounter with a bump and the return of structured behavior, we carried out the following steps: (i) we used high-speed videos, run at 1/70 actual time, to identify the first frame where no part of the bump remained (complete combustion), and (ii), we ran a MATLAB

program calculated the time between that frame and the first frame where the local average of B_{ap} (calculated over 1000 frames) reached a value of within 5% of the average value of B_{ap} in the structured regime (calculated over the first 7000 frames, well before the bump).

Image Analysis and Particle Tracking. To estimate the velocity of gases within nitrocellulose-fed flames, we developed a MATLAB program to determine the trajectory and speed of incandescent nitrocellulose particles within each flame. For each of 500 sequential images in a high-speed video of a propagating flame, this program (i) carried out a real space bandpass filter with noise and length settings optimized for the detection of incandescent particles of nitrocellulose, (ii) determined the centroid of each particle, (iii) tracked particles between adjacent flames, and (iv) determined the velocity of particles that could be tracked over ten frames (Fig. S8). The velocities used to calculate values of F_{thrust} and Fr_c^2, described below, represent the average of the ten fastest velocities for any given image set; these correspond the velocities of particles traveling close to the surface of the nitrocellulose strips.

Our estimates of particle velocities are based on images of the front of propagating flames (when viewed from the ignition end of the strip), and, thus, they approximate trajectories as being perpendicular to plane of the strip; as Figure S4B demonstrates, however, particles move at an acute angle relative to this plane. To estimate the error associated with such an approximation, we used a mirror to estimate particle velocities from two different orthogonal directions (Fig. S8G-I): the front of the flame, and the right side of the flame (90° to the front). For a 2.54-cm strip, estimates of particle velocities based on high-speed video of the front and side of the flame were 213 ± 6 cm/sec and 224 ± 12 cm/sec (n = 7 for both estimates), respectively; these two values differ by less than 10%.

Estimation of Froude Numbers (Fr_c^2). For flames, the convective Froude number (Fr_c^2) represents a metric for the relative contribution of inertial forces to buoyant forces to flame structure (Eq. S3) (2, 3); in Equation S3, U is the velocity of gases within the flame, ΔT is the temperature anomaly (the difference between the mean temperature of the flame and the temperature of the room), T is the temperature of the room, g is the acceleration due to gravity, and H is the height of the flame.

$$Fr_c^2 = \frac{U^2}{\frac{\Delta T}{T} \cdot g \cdot H} \qquad \text{(S3)}$$

We estimated values of Fr_c^2 for flames supported by strips of different widths and/or temperatures by employing image analysis (described above) to estimate U, high-speed images to estimate H, a thermal camera to estimate ΔT, and a digital thermometer and/or infrared thermometer (see "Experimental Setup") to estimate T.

SI Notes

SI Note 1. An Examination of Transport Phenomena Influencing Rates of Propagation.

For the structured regime, we assessed the contributions of (i) conductive heat flux into the support surface and (ii) oxygen flux out of the support surface by measuring rates of combustion along surfaces that differed in their thermal diffusivities and/or ability to permit oxygen transport to the bottom of the strip (Fig. S2). Rates of combustion proved insensitive to the composition of the support surface, but increased as restrictions to oxygen transport were lifted (no mesh to small mesh to large mesh). This last result, in light of the linear relationship between the rate of combustion and the width of the strips, suggests that restrictions on oxygen transport existed, but scaled with the width of the strips (and thus did not become more or less important as width was increased).

SI Note 2. Measurement of the Angle of Propagating Flames.

To assess how movements of the nitrocellulose strips could cause forward-bursting blasts (Fig. S4A), we tilted strips at various angles relative to a level surface (θ_{strip}), and examined the orientation of flames propagating along them (Fig. S4B).

We measured $\theta_{flame,}$ the angle between the flame and the surface of a strip, by (i) collecting high-speed images of structured flames propagating along strips positioned at various angles relative to a level surface (i.e., different values of θ_{strip}), and by (ii) using an angle measurement function of ImageJ to determine the angle between the front of the flame and the surface of the strip. The electrostatically charged strips stuck to the surface of the wire mesh for all values of θ_{strip}.

A plot of θ_{flame} vs. θ_{strip} shows that the orientation of a flame is dominated not by gravity, but by the inertia of gases leaving the strip and, thus, by the orientation of the strip (Fig. S4C). This result suggests that movements of the strip generate forward blasts of hot gases by tilting flames in the forward direction.

SI Note 3. Estimation of Buoyancy and Thrust.

For a 2.54-cm wide strip, we estimated the buoyant force that a structured flame burning on the underside of a strip exerts upward on that strip by carrying out the following steps: (i) we estimated T_{flame}, the average temperature of gases within the flame, by using thermal images; (ii) we estimated ρ_{flame}, the density of gases within the flame, by employing the ideal gas law (Eq. S4, where T_{air} is the temperature of ambient air in the room and ρ_{air} is the density of the bulk air);

$$\rho_{flame} = \frac{T_{air}}{T_{flame}} \rho_{air} \qquad \text{(S4)}$$

(iii) we estimated V_{flame}, the volume of the flame beneath the strip by using front and side images of the flame (V_{flame} = width of the strip x height of the flame x depth of the flame); and (iv) we estimated the buoyant force by employing Equation S5, where g is the acceleration due to gravity.

$$F_{buoyancy} = \left(\rho_{air} - \rho_{flame}\right) \cdot g \cdot V_{flame} \qquad \text{(S5)}$$

Values of V_{flame} and ρ_{fire} (Table S3) represent averages of measurements collected from at least three separate experiments. Fig. S6 shows images representative of those used to calculate (i) V_{flame} and (ii) T_{flame} (and, thus, ρ_{flame}).

For a 2.54-cm wide strip, we estimated the thrust that a structured flame burning on the underside of a strip exerts upward on that strip by multiplying the velocity of gases emanating from the surface of the strip by the mass flow rate of those gases (Eq. S6, where U is the velocity of incandescent particles of nitrocellulose within a structured flame burning upside down, ρ_{strip} is the density of the strip in g/cm^2, v is the velocity of the propagating flame in cm/s, and w_{strip} is the width of the strip in cm).

$$F_{thrust} = U \cdot \dot{m} = U \cdot (\rho_{strip} \cdot v \cdot w_{strip}) \qquad \text{(S6)}$$

At θ_{strip} = 180°, the structured flame was not stable and, thus, could only be imaged propagating over short distances; to facilitate measurement of its velocity, we used high-speed photography. Final values of U, ρ_{strip}, and v (Table S3) represent averages of measurements collected from at least three separate experiments. Fig. S6 shows images representative of those used to measure U and v.

Using the aforementioned approaches, we calculated values of $F_{buoyancy}$ and F_{thrust} of ~50 and ~140 μN, respectively. If we neglect drag on the paper strip and assume constant acceleration, we can calculate the time required for these forces to move a 1-cm stretch of strip over a distance of 1 cm by employing Equation S7, where Δx is the displacement (1 cm), and m is the mass of a 1-cm stretch of 2.54-cm wide strip.

$$t = \sqrt{\frac{2 \cdot \Delta x}{(F_{buoyancy} + F_{thrust})/m}} \qquad \text{(S7)}$$

Using the values in Table S3, we calculate t to be ~36 ms, a time similar to that over which we observe 1-cm movements of strip in videos (20-50 ms).

The estimates of buoyancy and thrust carried out in this section represent order-of-magnitude approximations. They indicate that the thrust and buoyant force exerted by a structured flame burning on the underside of a strip is sufficient to move that strip up, away from the wire mesh at speeds similar to those of the movements that we observe in the unstructured regime. Thus, they support our theory that upward movements of the nitrocellulose strips result from ignition of the underside of those strips.

SI Note 4. Forces Responsible for Causing Unstructured Flames to Shift Their Positions.

Back-and-forth movements of nitrocellulose strips suggest that unstructured flames shift their positions dynamically, constantly pushing the strips in different directions. High-speed videos of structured flames encountering the bump (1-cm inverted "V"), which exerts tension on the strip, reveal the forces responsible for such shifts (Movies S3 and S5). A 1-cm inverted "V" consists of three folds: one where the strip meets the front of the bump (fold 1, leftmost fold in Fig. 1B), one at the center of the bump (fold 2, central fold Fig. 1B), and one where the strip meets the back of the bump (fold 3, rightmost fold Fig. 1B); folds 1 and 3 exert tension on the strip (as they are folded in our procedure), tugging it upward. Prior to ignition of the strip, this tension is counteracted by the weight of the strip; as the flame burns away the mass holding the strip down, however, the tension exerted by fold 1 eventually pulls the strip upward (Fig. S7, 54 ms). As the strip moves away from the mesh, drag forces exerted by the air on the flame push it to the underside of the strip (Fig. S7, 99 ms). As the flame moves closer to the bump, buoyancy allows the flame to curl around to the top of the strip again (Fig. S7, 658 ms). Thus, in this system, flames move from one side of a strip to the other via (i) drag forces (i.e., wind, relative to the reference flame of the moving strip) and (ii) buoyant forces (in the case of bottom-to-top movements), thereby pushing strips in different directions.

SI Note 5. Mechanical Stiffness and the Unstructured Regime.

In the main text, we concluded that in the unstructured regime, propagating flames drive movements of the nitrocellulose strip and simultaneously shift their position in response to wind generated by those movements. To further examine this feedback loop, we tested the ability of structured flames to undergo structured-to-unstructured transitions while propagating along double-layer stacks (i.e., stacks of two strips, each containing a 1-cm inverted "V"). We hypothesized that these stacks, which are twice as thick—and, thus, twice as stiff—as single-layer strips, might be less responsive (in terms of movement) to the thrust and buoyant forces generated by unstructured flames; accordingly, this stiffness might obstruct the feedback loop that stabilizes the unstructured regime. To test this hypothesis, we first measured P_{SU} for the double-layer stack containing 1-cm bumps. Over 25 experiments, we observed no successful structured-to-unstructured transitions ($P_{SU} = 0$); we then examined high-speed videos for encounters under these conditions (Movie S6). These videos show that double-layer strips do, in fact, exhibit far less movement throughout the encounter than single-layer strips. These results are consistent with our hypothesis and suggest that the flexibility and energy density (lightness of the material supporting a flame of a given size) of nitrocellulose strips are key components of the feedback loop that stabilizes the unstructured regime.

SI Note 6. Examination of Oscillatory Behavior.

We examined the source of oscillations in B_{ap} by comparing plots in B_{ap} for structured and unstructured flames with corresponding high-speed videos and images. Figures S10A-10D show the different patterns of fluctuations associated with structured and unstructured flames. Figure S10A shows the stochastic fluctuations of a structured flame. Figure S10B shows oscillations resulting from oscillating asymmetry in the flame front. These oscillations are elaborated in Figures S10E-S10G. We define "oscillating asymmetry" to mean the oscillating angles between the wide dimension of the flame and the long dimension of the strip; by affecting the area of the flame exposed to the camera, these angles affect values of B_{ap}. Figure S10C shows oscillations resulting from the formation of convection cells that cause undulations in the height of the flame. Movie S1 shows these oscillations at 1/70 their actual speed (they also appear in the beginning of Movie S3). In general, oscillations in B_{ap} resulting from the formation of convection cells had a smaller amplitude and higher frequency than oscillations in B_{ap} resulting from oscillating asymmetry of the flame front. For example, for a structured flame propagating along a 1.27-cm strip, oscillations resulting from convection cells had a frequency and amplitude of 18.8 ± 1.9 Hz and 0.04 ± 1, respectively, while oscillations resulting from oscillating asymmetry of the flame front had a frequency and amplitude of 3.2 ± 0.7 Hz and 0.10 ± 0.04, respectively (n = 10). Figure S10D shows aperiodic oscillations associated with the random movements of unstructured flames. Figure S11 shows different patterns of fluctuations in B_{ap} for structured flames; plots correspond to nine experiments conducted under the same set of conditions. In the main text, when we refer to "irregular oscillatory behavior" in reference to structured flames, we are referring to the transient, irregular, or unpredictable appearance of oscillations caused by oscillating asymmetry in the flame front and/or by the formation of convection cells. Such oscillations appear in some, but not all, of the plots in Figure S11.

SI References

1. Box GEP, Jenkins GM, Reinsel GC (1994) *Time Series Analysis: Forecasting and Control* (Prentice Hall, Englewood Cliffs, NJ). 3rd Ed.

2. Drysdale D (1999) *An Introduction to Fire Dynamics* (Wiley, New York).

3. Clark TL, Jenkins MA, Coen J, Packham D (1996) A Coupled Atmosphere Fire Model: Convective Feedback on Fire-Line Dynamics. *J Appl Meteorol* 35:875–901.

SI Tables

Table S1. Probabilities of transitions under different conditions.

Condition	Transition*	Width of strip (cm)	Probability
Large Mesh** (20°C)	SU	1.27	0
	SU	2.54	0.74(0.06)
	SU	3.81	0.96(0.04)
	US	2.54	0.04(0.04)
Small Mesh** (20°C)	SU	2.54	0.68(0.07)
	SU	3.81	0.72(0.09)
	US	2.54	0.22(0.07)
Large Mesh (90°C)	SU	1.27	0.36(0.1)
	SU	2.54	1.0
Glass (20°C)	SU	1.27	0
	SU	2.54	0.04 (0.04)

*SU: structured-to-unstructured, US: unstructured-to-structured.
**Large and small meshes are described in detail in SI Methods.

Table S2. Rate of combustion for strips of different widths.

Width (cm)	Rate of combustion (g/s)	
	Structured	Unstructured
0.64	0.012 (0.001)	
1.27	0.019 (0.002)	
1.91	0.023 (0.002)	0.13 (0.01)
2.54	0.030 (0.002)	0.22 (0.01)
3.18	0.036 (0.002)	0.33 (0.05)
3.81	0.046 (0.003)	0.45 (0.06)
4.45	0.051 (0.004)	0.58 (0.11)
5.08	0.060 (0.004)	0.75 (0.11)

Table S3. Parameters used to estimate thrust and buoyancy.

Parameter	Estimated Value
U	271(61) cm/sec
ρ_{strip}	4.9 (0.1) g/cm^2
v	4.0(0.5) cm/s
T_{air}	20 °C
T_{flame}	200 °C
ρ_{air}	1.21
ρ_{flame}	0.75
g	9.82 cm/s^2
V_{flame}	12.05 cm^3
F_{thrust}	137 μN
$F_{buoynacy}$	54 μN

SI Figures

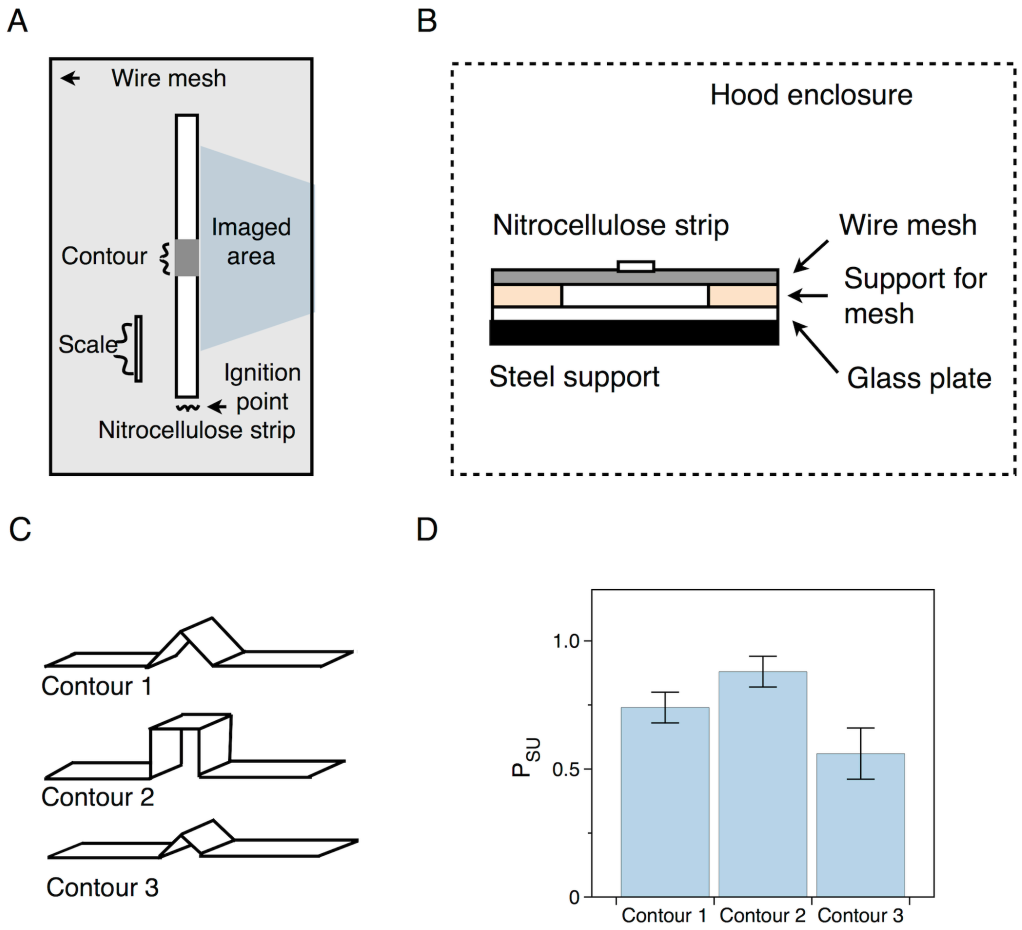

Fig. S1. Experimental setup. (A) We placed strips of nitrocellulose (with a length of 30 cm, a thickness of 140 μm, and widths ranging from 0.5 to 5 cm) onto a suspended wire mesh, and ignited them from one end. A 10-cm tall piece of cellulose paper, present in every image (scale), allowed us to determine pixel/length calibrations; from these calibrations, we added scale bars to each image. (B) Plastic petri dishes (pink) held the corners of the wire mesh 2.5 cm above a glass support surface (white), and an airflow-free fume hood (dashed lines) minimized interference by stray convective currents. (C) Several different bumps: a 1-cm inverted "V" (contour 1), a 1-cm square bump (contour 2), a 0.5-cm inverted "V" (contour 3). (D) The probability of a structured-to-unstructured transition for the three contours shown in (C). Error bars indicate the standard error of the probability ($n \geq 25$).

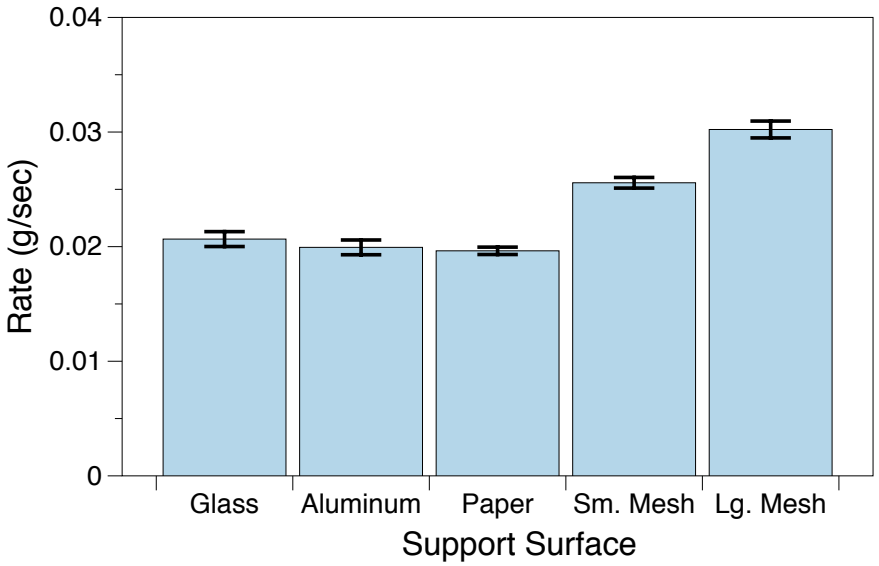

Fig. S2. Rates of combustion for structured flames propagating along strips supported by different materials. Flames traveled along 2.54-cm strips. The small mesh contains diamond-shaped holes with areas of 0.051 cm^2 and a density of ~ 5 holes/cm^2. The large mesh contains diamond-shaped holes with areas of 0.13 cm^2 and a density of ~ 2 holes/cm^2. The holes account for ~25% of each mesh (by area). Error bars represent standard error ($n \geq 5$).

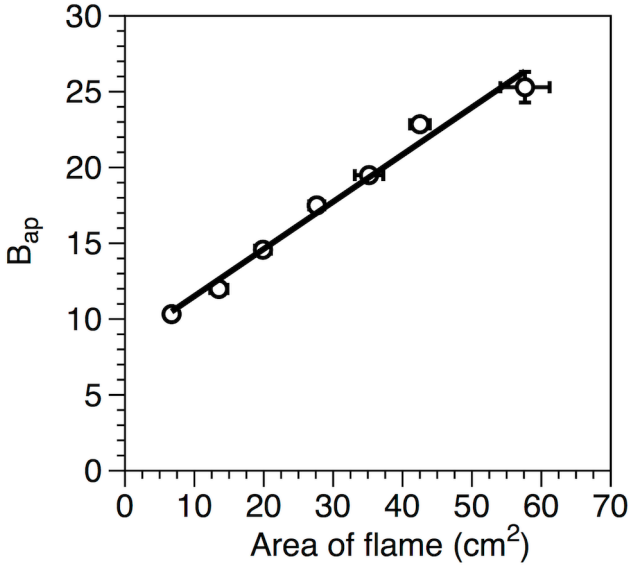

Fig. S3. The dependence of B_{ap} on the area of a flame. Values of B_{ap} and area were estimated for flames supported by strips of different widths. Values of B_{ap} increase linearly with the area of a flame (slope = 0.31 cm^{-2}, $r^2 = 0.98$). Error bars indicate standard error ($n \geq 5$).

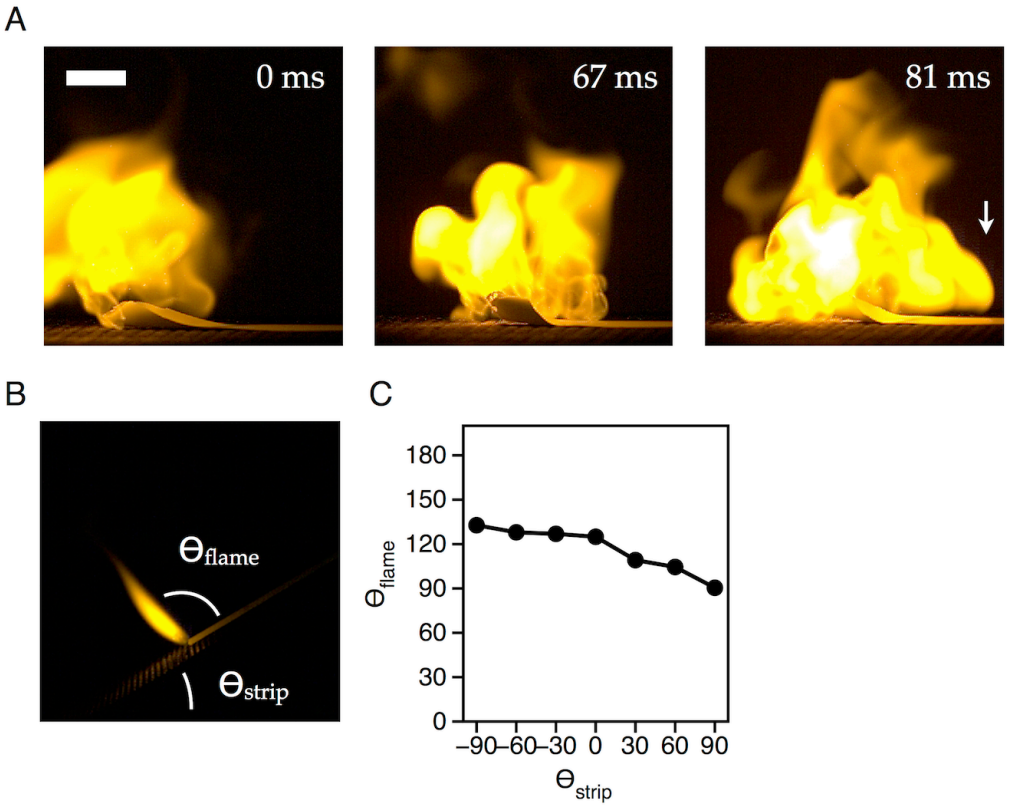

Fig. S4. (A) Convective blasts generated by movements of the strip. Still frames from a high-speed video of an unstructured flame show how movements of the strip drive blasts of hot gases that extend forward over the surface of the strip (white arrow). Scale bar = 2 cm. (B) A high-speed image showing a structured flame propagating along a 2.54-cm strip positioned at 30° relative to a level surface (θ_{strip} = 30°). (C) Relationship θ_{strip} and the angle between the flame and the surface of the strip (θ_{flame}).

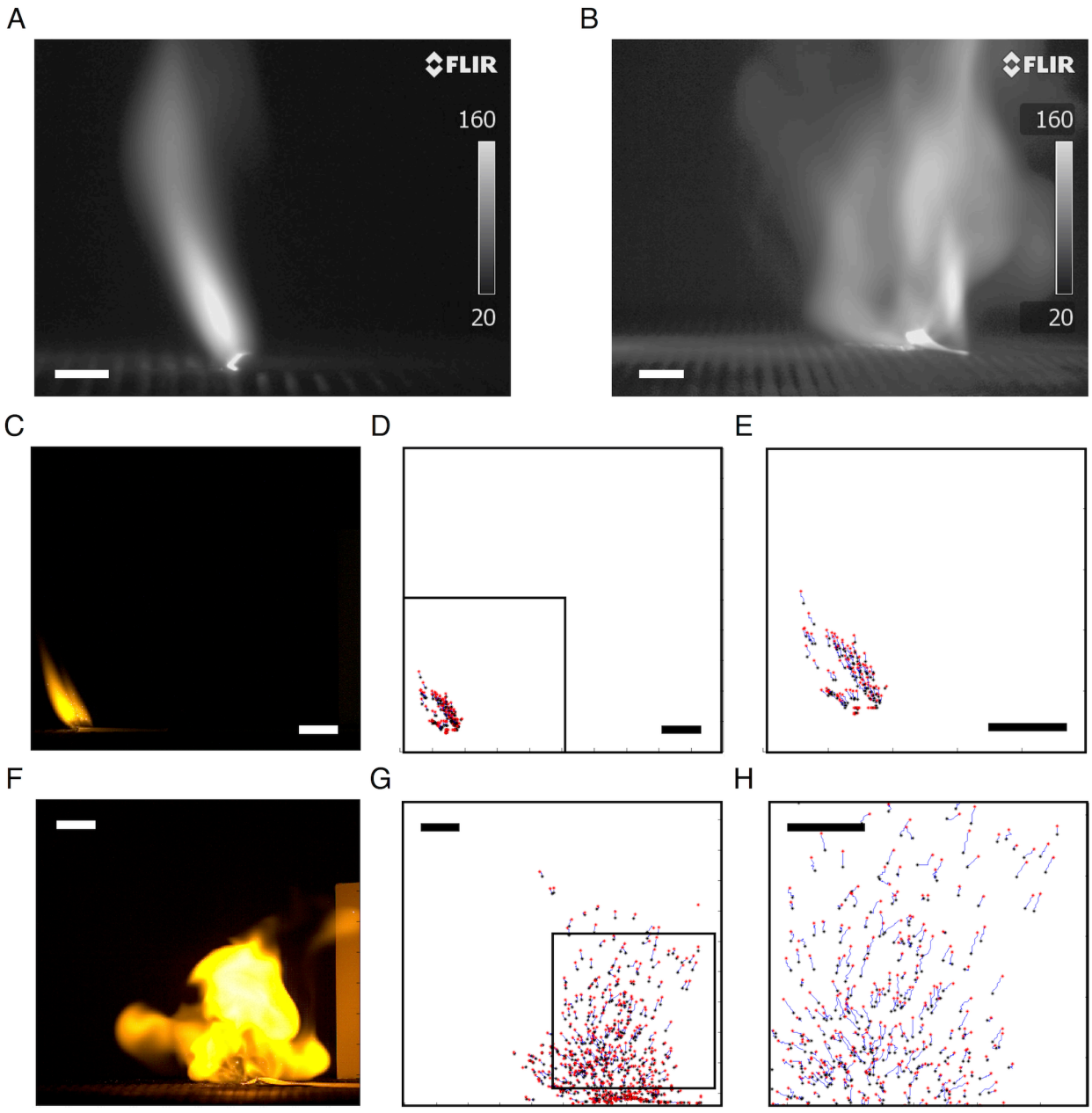

Fig. S5. Structured and unstructured flames. (A) An infrared image of a structured flame propagating along a 2.54-cm wide strip. Hot gases extend beyond a sharply delineated region of ignited nitrocellulose. (B) An infrared image of an unstructured flame traveling along a 2.54-cm wide strip. Hot gases extend beyond a region of ignited nitrocellulose that is much larger than the corresponding region of the structured burning regime. In (A) and (B) the temperature scale was fixed at a maximum of 160°C to optimize the visibility of hot gases within the flames. (C) High-

speed image of a structured flame. (D) Trajectories of incandescent particles of nitrocellulose tracked from 36 ms before the image in C to 36 ms after. (E) Detail of trajectories shown in D; particles move roughly parallel to one another. (F) High-speed image of an unstructured flame. (G) Trajectories of incandescent particles of nitrocellulose tracked from 36 ms before the image in F to 36 ms after. (H) A detail of the trajectories in G; trajectories radiate outward in many directions, including the direction of propagation. Scale bars in (A-H) represent 2 cm.

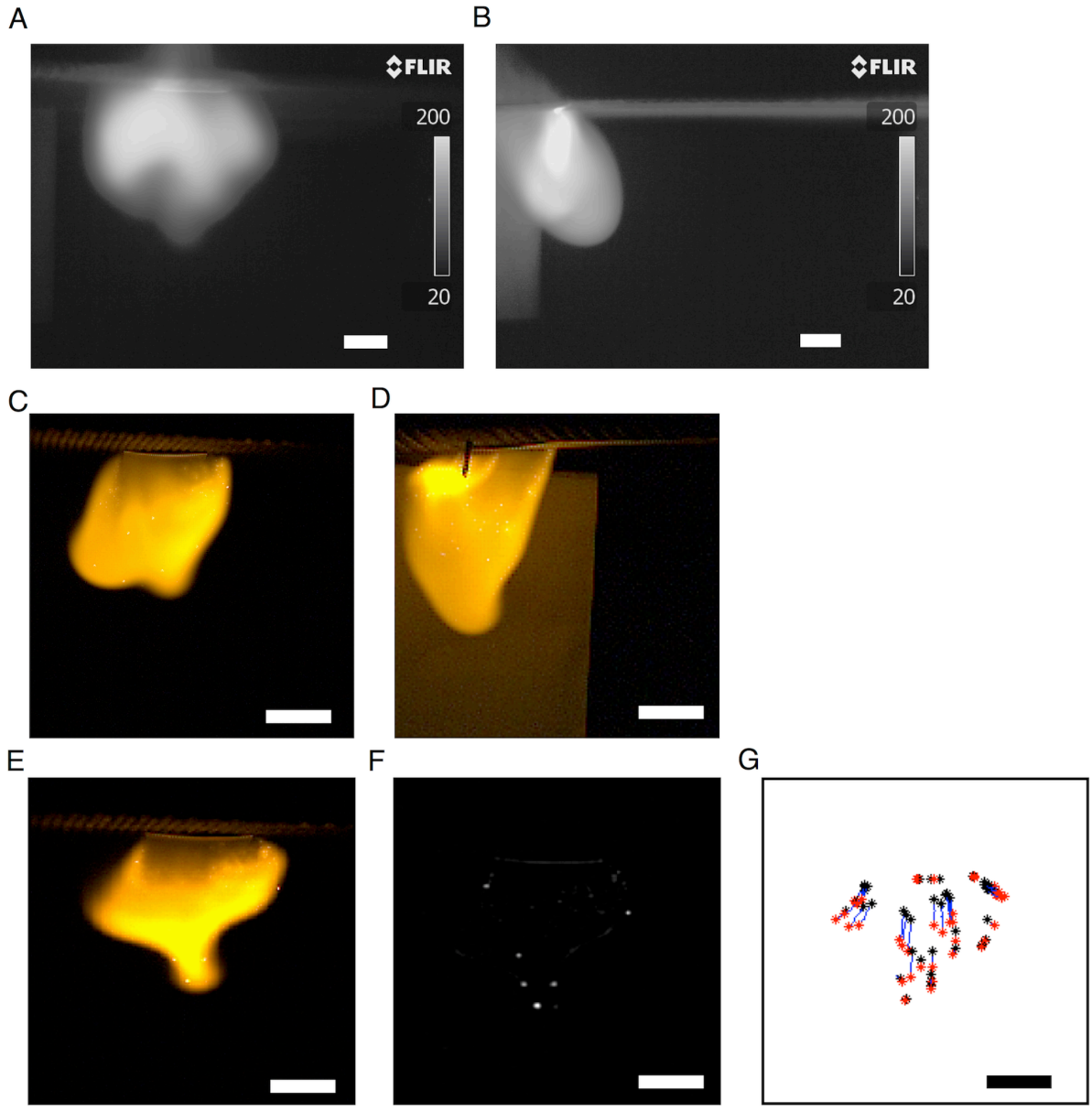

Fig. S6. Images of a structured flame burning upside down. For (A-G), θ_{strip} = 180° and W_{strip} = 2.54-cm. (A) Thermal image of the front of the flame (propagating away from the camera). (B) Thermal image of the side of the flame (propagating from left to right). (C) High-speed image of the front of the flame (propagating away from the camera). (D) High-speed image of the side of the flame (propagating left to right). (E) High-speed image of the front of the flame. (F) Filtered image of the front of the flame showing incandescent particles of nitrocellulose. (G) Particle trajectories. (A-G) Scale bars = 1 cm.

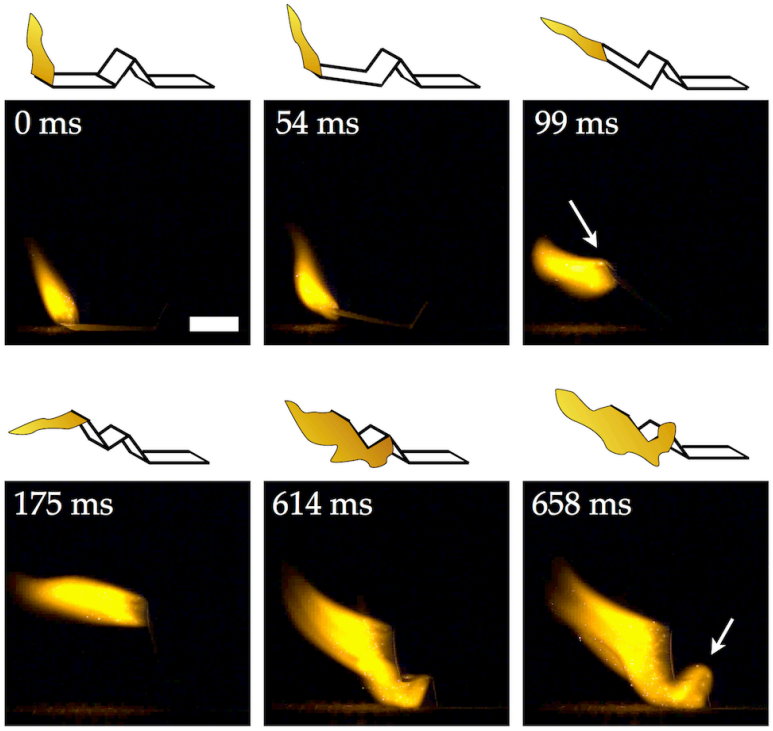

Fig. S7. High-speed images of a structured flame encountering a 1-cm inverted "V". As the flame approaches the bump, tension in the bump raises the paper up (54 ms), exposing the flame to wind, which pushes it to the underside of the strip (99 ms, white arrow). As the flame spreads further into the bump (614 ms), buoyant forces push part of the flame back to the top of the strip (658 ms, white arrow).

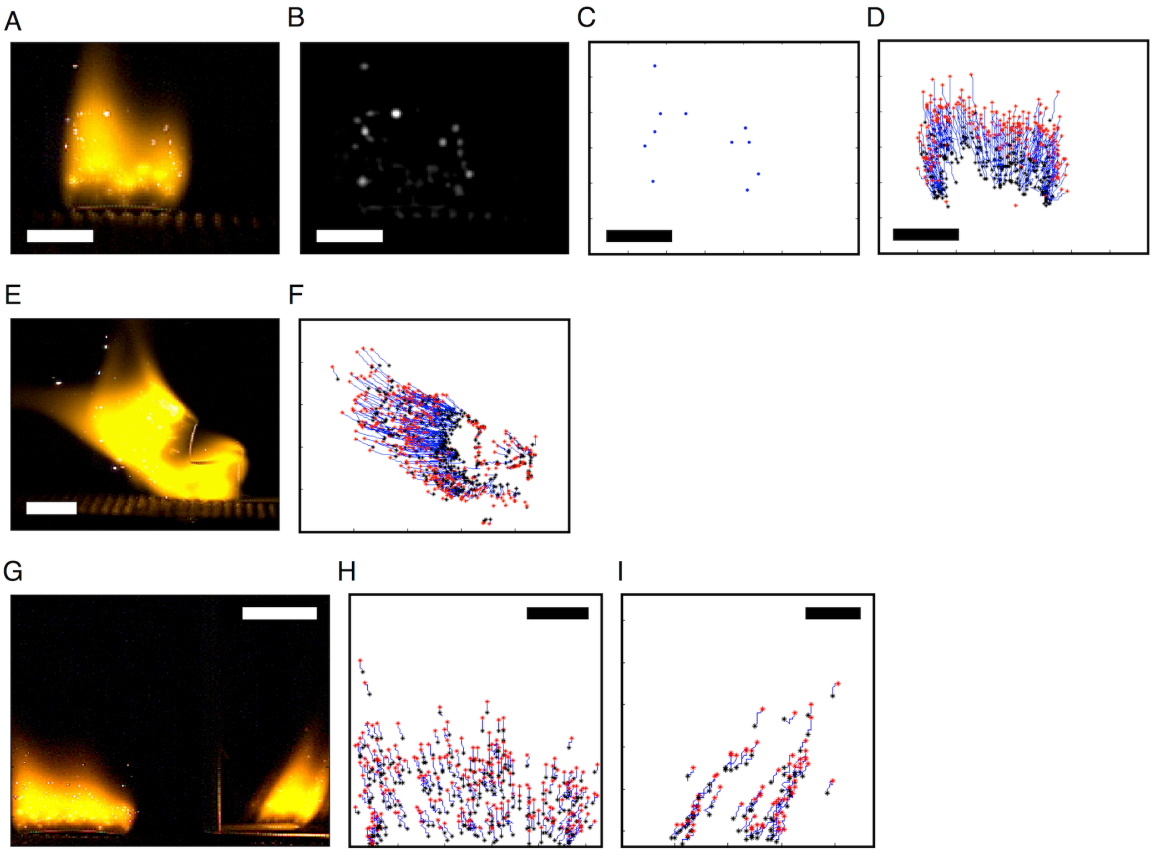

Fig. S8. Details of image analysis. (A-D) Steps for calculating the velocity of gases within nitrocellulose-fed flames (scale bar = 1 cm): (A) we captured high-speed images of structured flames, (B) subjected those images to a real-space bandpass filter optimized to isolate nitrocellulose particles, (C) identified the centroid of each particle, and (D) plotted the trajectories of those particles over 500 successive frames (right). (E-F) A structured-to-unstructured transition (scale bar = 1 cm): (E) high-speed image, and (F) trajectories of particles (right). (G-I) Analysis of gas velocities from two orthogonal directions: the front of the flame, and the right side of the flame (90° to the front). Figures are as follows: (G) a structured flame supported by a 2.54-cm strip (left side of image), and the reflection of that flame in a mirror angled 45° relative to the long dimension of the strip (right side of image; scale bar = 2 cm), (H) trajectories of particles imaged from the front of the flame (scale bar = 1 cm), and (I) trajectories of particles imaged from the right side of the flame (scale bar = 1 cm).

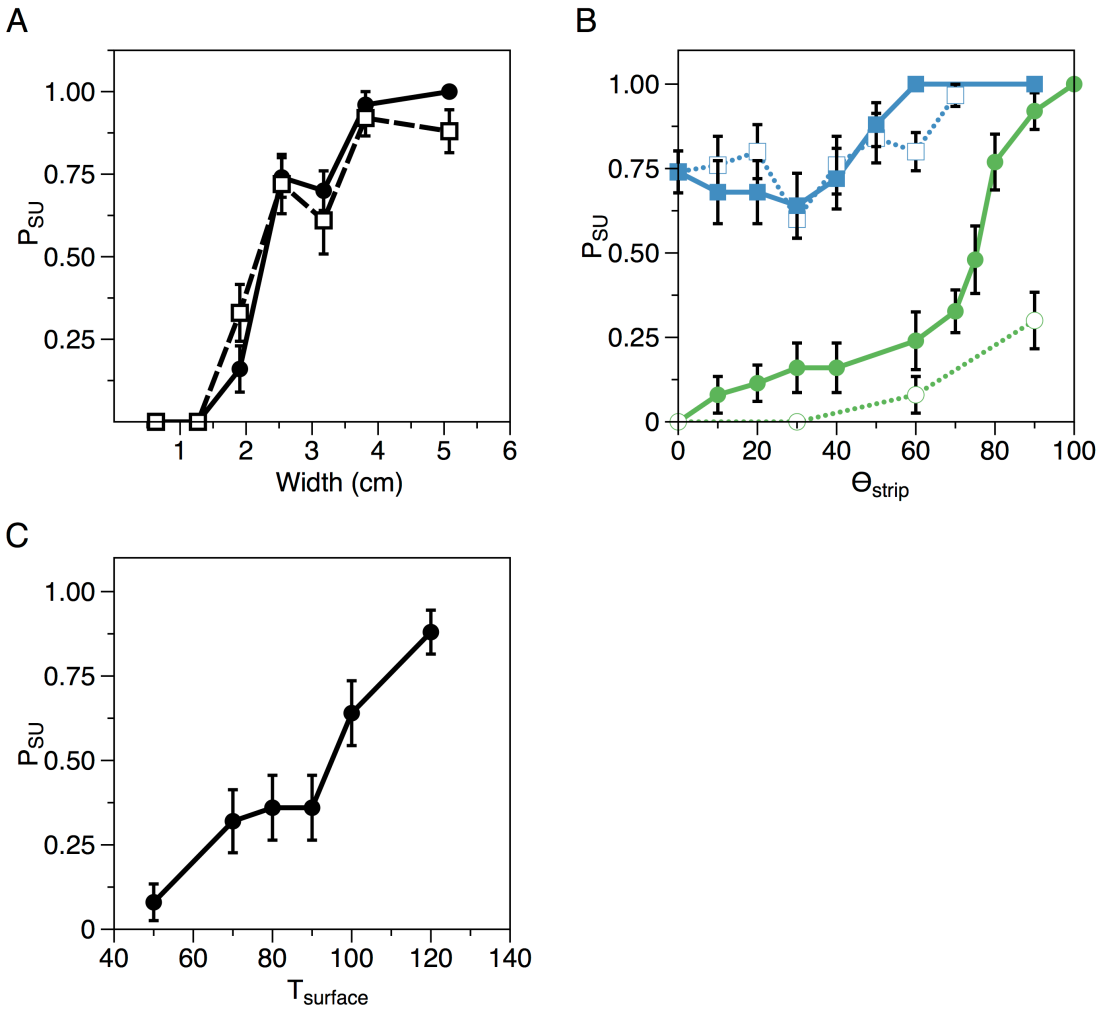

Fig. S9. The influence of the width of the strips and the slope and temperature of the mesh supporting them on P_{SU}. (A) A plot showing values of P_{SU} for flames propagating along strips of different widths; points represent values of P_{SU} estimated from different batches of nitrocellulose: batch 1 (closed circle, ●, solid line) and batch 2 (open square, □, dashed line). (B) A plot showing values of P_{SU} for flames propagating up (solid lines) and down (dotted lines) strips tilted at various angles relative to a level surface (θ_{strip}). Colors correspond to different widths of strip: 2.54 cm (blue) and 1.27 cm (green). (C) A plot showing values of P_{SU} for flames propagating along 1.27-cm strips supported by surfaces (the large mesh as defined in SI Methods) at different temperatures. Error bars in (A-C) represent standard error ($n \geq 25$).

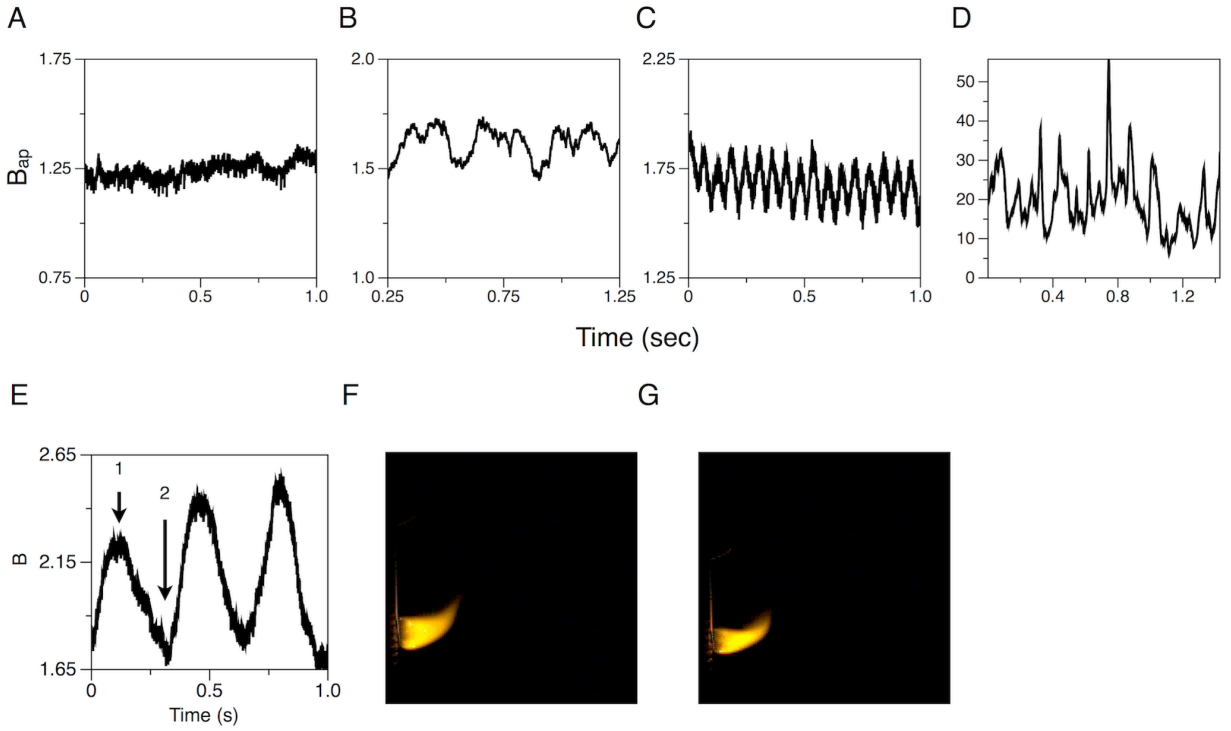

Fig. S10. Examples of fluctuations in B_{ap}. (A-D) Mean values of B_{ap} for sequential high-speed images of (A) a structured flame, (B) a structured flame exhibiting periodic oscillations caused by oscillating asymmetry in the flame front (1.27-cm strip, large mesh, 90°C), (C) a structured flame exhibiting periodic oscillations caused by the formation of convection cells (2.54-cm strip, small mesh), and (D) an unstructured flame exhibiting aperiodic oscillations caused by cyclic convective blasts of hot gases (2.54-cm strip, small mesh). (E) The mean apparent brightness (B_{ap}) of a structured flame propagating along a 1.27-m strip positioned at 90° relative to a level surface (θ_{strip} = 90°). (F) A high-speed image of the flame at position 1 in (E). (G) A high-speed image of the flame at position 2 in (E). (F-G) As the angle between the wide dimension of the flame and the long dimension of the strip changes, the area of the flame exposed to the camera, which is reflected in the magnitude of B_{ap}, responds accordingly.

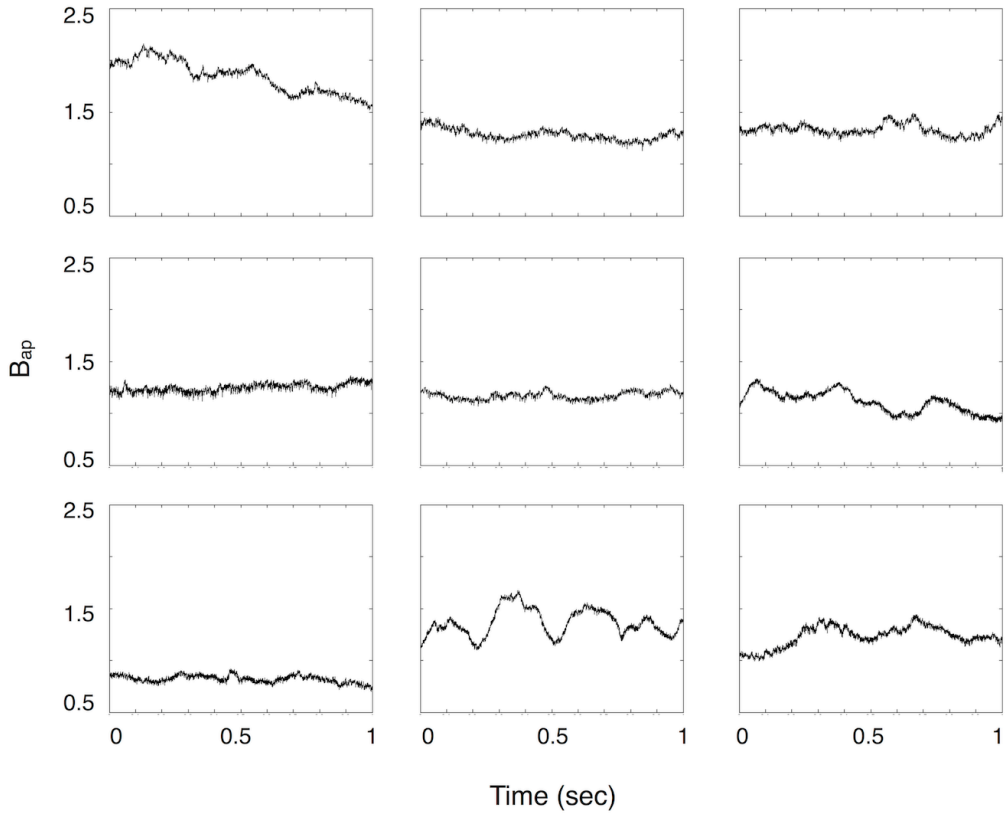

Fig. S11. Variability in B_{ap} for a single set of conditions. Plots show the evolution of mean apparent brightness (B_{ap}) of a structured flame propagating up a 1.27-cm strip positioned at 40° relative to a level surface ($\theta_{strip} = 40°$). Variability between the plots arises from the irregular nature of oscillatory fluctuations.

SI Movie Legends.

In all videos, the thin strip of paper on the left side of the screen serves as a 10-cm scale bar.

Movie S1. A structured flame (1/70 actual speed). In this video, a structured flame propagates along a 2.54-cm wide strip of nitrocellulose (large mesh).

Movie S2. An unstructured flame (1/70 actual speed). In this video, an unstructured flame propagates along a 2.54-cm wide strip of nitrocellulose. A 1-cm triangular bump, positioned 4 cm from the point of ignition, generated this flame by triggering a structured-to-unstructured transition.

Movie S3. A structured-to-unstructured transition (1/10 actual speed). A 1-cm triangular bump, positioned 13 and 15 cm from the ignition and extinction ends of a 2.54-cm wide strip (large mesh), respectively, triggers this transition.

Movie S4. An unstructured-to-structured transition (1/10 actual speed). A 1-cm triangular bump, positioned 4 cm from the ignition end of a 2.54-cm wide strip (small mesh), triggered the initial unstructured flame. In the video, a second bump, positioned 14 cm away from the first (8 cm from the extinction end of the strip) triggers the unstructured-to-structured transition.

Movie S5. An structure-to-unstructured transition followed by an unstructured-to-structured transition (1/10 actual speed). A 1-cm triangular bump, positioned 13 cm away from the ignition end of a 2.54-cm wide strip (small mesh) triggers the first transition (structured-to-unstructured). A second bump, positioned 5 cm away from the first (and 8 cm away from the end of the strip), triggers the second transition (unstructured-to-structured).

Movie S6. A failed structured-to-unstructured transition on a double-layer strip (1/10 actual speed). A flame propagating along a stack of two 2.54-cm wide strips (large mesh) containing a 1-cm triangular bump.